Nano Research
2019, 12(3): 563–568

ISSN 1998-0124 CN 11-5974/O4
https://doi.org/10.1007/s12274-018-2254-y

Research Article

Doping modulated in-plane anisotropic Raman enhancement on layered ReS_2

Na Zhang[1], Jingjing Lin[1], Shuqing Zhang[1], Shishu Zhang[1], Xiaobo Li[2], Dongyan Liu[2], Hua Xu[2], Jin Zhang[1], and Lianming Tong[1] (✉)

[1] *Center for Nanochemistry, Beijing Science and Engineering Center for Nanocarbons, Beijing National Laboratory for Molecular Sciences, College of Chemistry and Molecular Engineering, Peking University, Beijing 100871, China*
[2] *School of Materials Science and Engineering, Shaanxi Normal University, Xi'an 710119, China*

Received: 13 September 2018 / **Revised:** 11 November 2018 / **Accepted:** 25 November 2018

ABSTRACT

Anisotropic two-dimensional (2D) materials exhibit lattice-orientation dependent optical and electrical properties. Carriers doping of such materials has been used to modulate their energy band structures for opto-electronic applications. Herein, we show that by stacking monolayer rhenium disulfide (ReS_2) on a flat gold film, the electrons doping in ReS_2 can affect the in-plane anisotropic Raman enhancement of molecules adsorbed on ReS_2. The change of enhancement factor and the degree of anisotropy in enhancement with layer number are sensitively dependent on the doping level of ReS_2 by gold, which is further confirmed by Kelvin probe force microscopy (KPFM) measurements. These findings could open an avenue for probing anisotropic electronic interactions between molecules and 2D materials with low symmetry using Raman enhancement effect.

KEYWORDS

ReS_2, anisotropy, charge transfer, Raman enhancement, electrons doping

1 Introduction

Anisotropic two-dimensional (2D) materials, such as black phosphorous (BP) [1–3], stannic selenide (SnSe) [4, 5] and rhenium disulfide (ReS_2) [6–8], have drawn enormous attention due to not only their advantageous electrical and optical properties but also their unique anisotropy. For example, owing to the different effective mass of the electrons and holes, the carrier mobility and conductivity along different crystalline axes are different [9, 10]. The optical and spectroscopic characteristics, including absorption [11–14], photoluminescence [15, 16], and Raman scattering [17–21], are also sensitively dependent on the direction of light polarization with respect to the crystalline orientation. Such anisotropic properties have been extensively studied and are beneficial for polarization-dependent optoelectronic detectors [22–27].

ReS_2 is a low-symmetrical 2D crystal with triclinic crystal structure where the neighboring Re atoms are linked along the *b* [010] axis to form Re diamond-shape (DS)-chains [6, 28–30]. Unlike vulnerable BP, it exhibits good stability in air [31]. It maintains direct bandgap from monolayer to bulk [32], and has shown great potential as field effect transistors, digital inverters and photodetectors [22, 33, 34]. Besides, ReS_2 can enhance the Raman scattering of molecules adsorbed on the surface, which exhibits anisotropic enhancement depending on the lattice orientation of ReS_2 [35, 36].

A number of studies reported the doping of anisotropic 2D materials either by heteroatoms [37–39], molecules [40] or another 2D material [41, 42]. For example, heteroatom doping was performed to tune BP from a moderate-gap semiconductor to a band-inverted semimetal [38]. The doping from electron-donor and electron-acceptor molecules could remarkably affect the electronic and optical properties of BP [40]. A chloride molecular doping technique of the few-layer WS_2 and MoS_2 was also reported, which greatly reduced the contact resistance in transition metal dichalcogenides (TMDs)-based nanoelectronic devices [43]. It was also reported that in BP/ReS_2 van der Waals heterostructures, a highly doped n^+/p^+ heterojunction formed and was used as a negative differential resistance (NDR) device [41].

Herein, we report that by depositing a thin gold film on layered ReS_2 of different layer numbers, in-plane anisotropic Raman enhancement of probing molecules on the surface of ReS_2 disappeared due to the electrons doping of ReS_2 by gold. The enhanced Raman scattering of molecules by intrinsic ReS_2 was angular dependent due to the different charge transfer probabilities between ReS_2 and molecules oriented along different crystalline directions [35]. However, the angular dependence of Raman enhancement disappeared when ReS_2 was in contact with the gold film, and the enhancement factor decreased, indicating isotropic probability of charge transfer between molecules and doped monolayer ReS_2, that is, the decrease probability of charge transfer from highest occupied molecular orbital (HOMO) of copper phthalocyanine (CuPc) to the conduction band of ReS_2 due to the electrons doping by gold. Furthermore, with the increasing layer number of ReS_2, the angular dependence gradually appeared and recovered to that of intrinsic ReS_2. Kelvin probe force microscopy (KPFM) confirmed the different degree of doping in monolayer and few-layer ReS_2 on gold. Monolayer ReS_2 was also transferred onto monolayer graphene, and the decrease of anisotropy of Raman enhancement was also observed.

Address correspondence to tonglm@pku.edu.cn

2 Results and discussion

Monolayer ReS_2 was prepared by mechanical exfoliation onto a clean 300 nm SiO_2/Si substrate. Figures 1(a) and 1(b) show the optical microscopy (OM) and atomic force microscopy (AFM) images. The thickness was measured to be 1.2 nm, corresponding to monolayer of ReS_2 [44]. CuPc molecules were deposited on the sample using thermal vacuum deposition (see the Experimental section). The enhanced Raman scattering of CuPc was clearly observed in Fig. 1(c), where the enhancement factor was ~ 8 when the laser polarization was parallel to *b*-axis. The dominant enhancement of nontotally symmetric modes (B_{1g} modes at 748, 1,343, 1,530 cm^{-1}) strongly indicates the occurrence of charge transfer [45]. Angle-resolved polarized Raman spectroscopy (ARPRS) was performed under parallel polarization configuration to study the polarization dependence of the enhanced Raman spectra. As shown in Figs. 1(d)–1(h), the Raman intensities of both ReS_2 (Fig. 1(d)) and CuPc (Fig. 1(e)) change periodically with sample rotation angles, and the polar plots of the Raman intensity of both the A_g-like mode of ReS_2 at 212 cm^{-1} (Fig. 1(f)) and Raman modes of CuPc at 1,450 cm^{-1} (B_{2g}, Fig. 1(g)) and 1,530 cm^{-1} (B_{1g}, Fig. 1(h)) showed periodicity of 180° and 90°, respectively [46–49]. It is also seen that the corresponding angle of maximum intensity of ReS_2 (212 cm^{-1}) coincides with the B_{1g} mode of CuPc at 1,530 cm^{-1}, which indicates that the molecules with major axes parallel to the *b*-axis of ReS_2 contributed to the majority of Raman enhancement with the highest probability of charge transfer [35, 36, 45, 50, 51].

By depositing a thin film of gold on ReS_2, the doping of electrons in ReS_2 can lead to charge redistribution, which can be probed by the in-plane anisotropic Raman enhancement of ReS_2 to CuPc molecules. Figure 2 illustrates the preparation of monolayer ReS_2 on the top of a gold film of 40 nm thickness (see Experimental section). Sub-monolayer of CuPc molecules was then deposited on the as-prepared sample for Raman measurements.

Figure 3(a) shows the AFM image of monolayer ReS_2 on mica substrate. After the deposition of 40 nm Au on ReS_2, it is seen that the surface of the gold film is rather flat with RMS of less than 1 nm (Fig. S1 in the Electronic Supplementary Material (ESM)) [52]. ReS_2 on the gold film also exhibited Raman enhancement to CuPc molecules, as shown in Fig. 3(b). The black curve shows the Raman spectrum of CuPc on gold film, and the intensity was slightly lower than that on SiO_2/Si substrate (Fig. S2 in the ESM), indicating negligible electromagnetic enhancement from gold due to the smoothness of the surface [53]. The Raman spectrum of CuPc on ReS_2 (red curve) shows higher intensity. The enhancement factor (the ratio of intensity of CuPc molecules on ReS_2/Au/SiO_2/Si compared with that on Au/SiO_2/Si, ~ 2.3) is lower than that on SiO_2/Si substrate without gold film. This can be attributed to the modulation of energy band of ReS_2 by gold, and the energy band alignment between ReS_2 and CuPc molecules, which will be discussed later. From the angular dependence of Raman spectra of ReS_2 in Figs. 3(c) and 3(e), it can be inferred that ReS_2 remained its crystalline anisotropy, that is, the structure of ReS_2 was not changed by the deposition of gold. The intensity was lower than that on SiO_2/Si substrate due to the lack of interference enhancement from SiO_2. Nevertheless, the polar plot

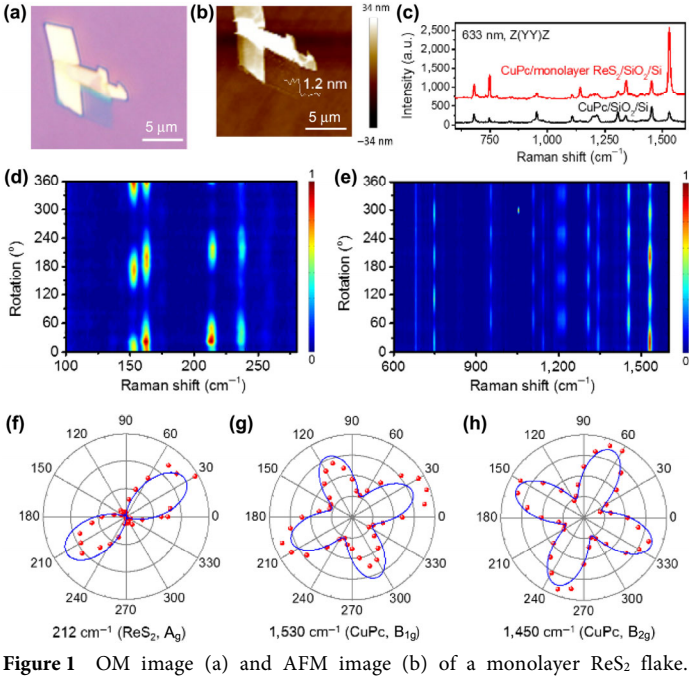

Figure 1 OM image (a) and AFM image (b) of a monolayer ReS_2 flake. (c) Raman spectra of CuPc molecules on a 300 nm SiO_2/Si substrate with (red) and without (black) monolayer ReS_2. Angular dependence of the normalized Raman spectra of ReS_2 (d) and CuPc molecules on ReS_2 (e), respectively. (f)–(h) Polar plots of the normalized intensities of 212 cm^{-1} (ReS_2, A_g), 1,530 cm^{-1} (CuPc, B_{1g}), 1,450 cm^{-1} (CuPc, B_{2g}) modes as a function of sample rotation angle on ReS_2.

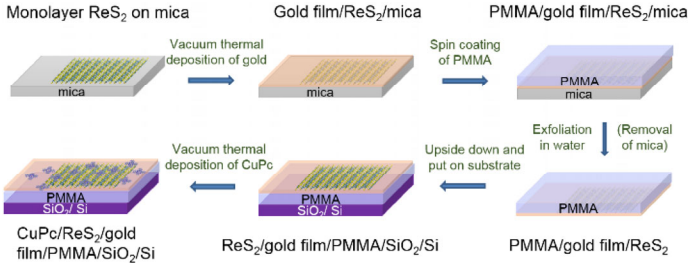

Figure 2 Schematic illustration of the sample preparation procedure of gold/ReS_2/CuPc molecules.

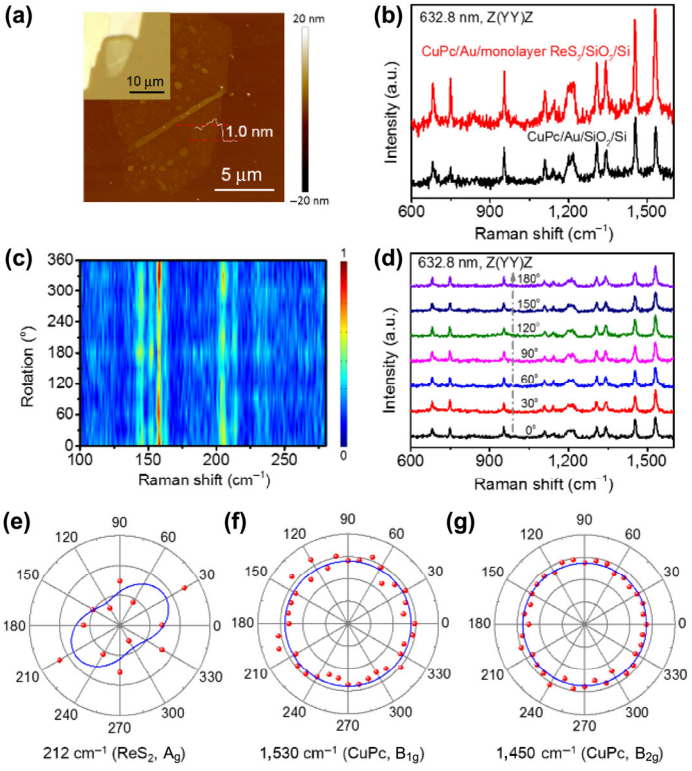

Figure 3 AFM (a) image of a monolayer ReS_2 flake with gold film underneath. The insert is the optical image of it. (b) Raman spectra of CuPc molecules on a Au/300 nm SiO_2/Si substrate with (red) and without (black) monolayer ReS_2 on top. (c) Angular dependence of the normalized Raman spectra of ReS_2. (d) Raman spectra of CuPc molecules on ReS_2. (e)–(h) Polar plots of the normalized intensities of 212 cm^{-1} (ReS_2, A_g), 1,530 cm^{-1} (CuPc, B_{1g}), 1,450 cm^{-1} (CuPc, B_{2g}) modes as a function of sample rotation angle measured on ReS_2.

clearly identified the *b*-axis of ReS_2. However, the Raman spectra of CuPc did not change with sample rotation angles, as shown in Figs. 3(d), 3(f) and 3(g). Neither the absolute intensities nor the relative intensities between different modes changed. The polar plots in Figs. 3(f) and 3(g) explicitly show circular patterns, in stark contrast to Figs. 1(g) and 1(h).

The electrons doping of ReS_2 by gold was evidenced by the change of the peak positions and peak widths of the Raman scattering (Fig. S3 in the ESM) [54]. All Raman characteristic peaks showed slight blueshift owing to the electrons doping [55]. The new peak at 157.0 cm^{-1} was attributed to the activation of the infrared-active modes due to the breaking of inversion symmetry caused by Au deposition, while the peak at 228.4 cm^{-1} could be attributed to double resonance processes involving M- or K-point phonons [56]. The peak around 200.0 cm^{-1} has not been reported and could be an indication of strong interaction between S and Au atoms. All the Raman characteristic peaks were broadened due to the modulation by gold, which is attributed to the injection of electrons in conduction band minimum (E_c) of ReS_2, which complicates the electron–photon interaction in Raman scattering process [57].

The doping was found to be layer-number dependent. For a bilayer ReS_2 on gold film, the Raman enhancement effect also occurred with slightly higher enhancement factor, as shown in Fig. 4(a). More importantly, Fig. S5 in the ESM showed that the angular dependence of the Raman enhancement also appeared but with weak anisotropy. With increasing layer number to trilayer (Fig. S6 in the ESM) and fewlayer (~ 5 nm) (Fig. S7 in the ESM), the Raman enhancement factor increased further (Fig. 4(a)), and the anisotropy became more apparent. The degree of anisotropy in enhancement, defined by the ratio of maximum and minimum intensities of the vibrational mode of CuPc at 1,450 cm^{-1}, is plotted in Fig. 4(b), which shows an increase with layer number.

KPFM measurement was performed to obtain the surface potential of ReS_2 on gold. The contact potential difference (ΔV_{CPD}) was defined as the difference between the substrate and the aluminum-coated tip. The tip was calibrated on a highly oriented pyrolytic graphite (HOPG) surface (work function 4.6 eV) [58], and the work functions of the tip and the gold surface were found to be 4.816 and 4.647 eV, respectively. The E_c, valence band maximum (E_v) and Fermi level (E_f) of ReS_2 were reported to be −4.05, −6.75 and −4.82 eV [41, 59], respectively, so the Fermi level was expected to be slightly lower than that of vacuum-deposited gold films [60, 61]. Figure 4(c) exhibits the three-dimensional KPFM mapping of the as-prepared ReS_2/gold heterostructure, and ΔV_{CPD} histograms extracted from the mapping image marked by arrow were plotted in Fig. 4(d), which show 160.5 and 142.4 mV for fewlayer (~ 5 nm) and multilayer (> 10 nm) ReS_2 flakes, respectively. It can be figured that the work function of fewlayer ReS_2 (4.809 eV, see Experimental section) was lower than that of multilayer ReS_2 (4.827 eV), and the latter held almost the same value as pristine ReS_2 [59]. Accordingly, Fig. 4(e) shows the energy band structure of ReS_2/gold, where electrons transferring from the Fermi level of gold to E_c of ReS_2 can be seen and leads to increased electrons density in E_c. Since the charge transfer occurs between the HOMO of CuPc (−5.2 eV) and E_c of ReS_2 [62], the increase of electrons density in E_c decreased the probability of charge transfer from CuPc molecules with major axes parallel to the *b*-axis of ReS_2. As a result, the average enhancement factor (~ 2.3 vs. ~ 8.0 for monolayer ReS_2 on gold vs. silica) was decreased, and at the same time, the angular dependence also disappeared. The increase of work function of ReS_2 with increasing layer number also suggested energy alignment with CuPc molecules and larger enhancement factor. On the other hand, less electrons doping in E_c of ReS_2 and larger probability of charge transfer led to the increase of degree of anisotropy, as shown in Fig. 4(b). This is consistent with the ground-state coupling between CuPc molecules and ReS_2 [45, 51], as shown in Fig. 4(f).

By replacing gold film with monolayer graphene (schematics in Fig. 5(a)), the Raman enhancement of CuPc molecules by ReS_2 was

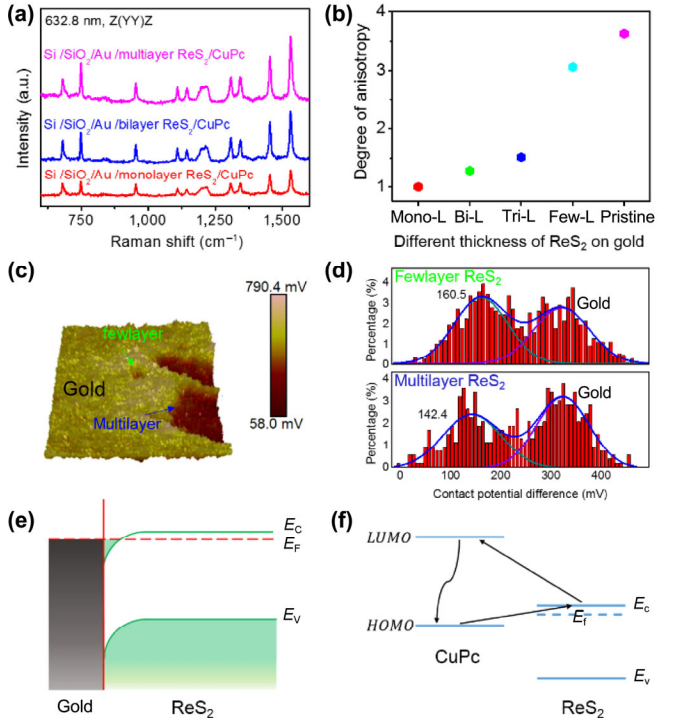

Figure 4 (a) Raman spectra of CuPc molecules on ReS_2/gold film/PMMA/300 nm SiO_2/Si substrate. (b) Degree of anisotropy in enhancement as a function of layer numbers of ReS_2 on gold film. (c) Three-dimensional KPFM mapping of the ReS_2/gold heterostructure. Fewlayer and multilayer ReS_2 were indicated by green and blue arrows, respectively. (d) Histogram distributions of ΔV_{CPD} of fewlayer (up) and multilayer (down) ReS_2 extracted from the KPFM mapping image. (e) Energy band alignments of ReS_2 and gold at equilibrium. (f) Energy band alignments of CuPc molecules and ReS_2.

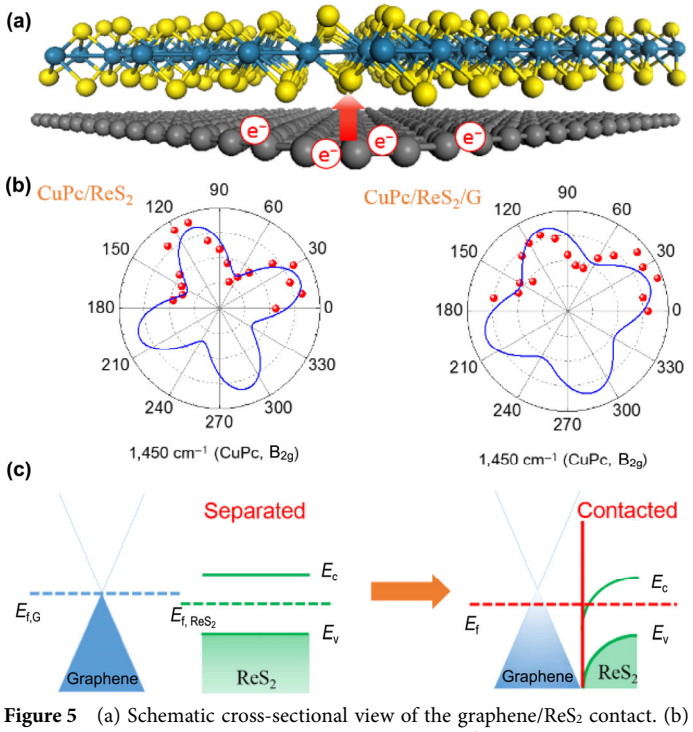

Figure 5 (a) Schematic cross-sectional view of the graphene/ReS_2 contact. (b) Polar plots of the normalized intensities of 1,450 cm^{-1} (CuPc, B_{2g}) modes as a function of sample rotation angle measured on ReS_2 contact without (left) and with (right) graphene. (c) Energy band alignments of ReS_2 before and after the contact with graphene.

also observed with an enhancement factor of 2.8, which is lower than that on pure ReS_2. The degree of anisotropy of peak 1,450 cm^{-1} was found to be 1.6, as shown in Fig. 5(b). The G' band of graphene covered by ReS_2 redshifted from 2,695.6 to 2,706.6 cm^{-1} (Fig. S9(b) in the ESM), indicating p-doping by ReS_2 [63], i.e., electrons transfer from graphene to ReS_2. The energy band alignments of graphene and ReS_2 are shown in Fig. 5(c).The Fermi level of graphene downshifted as the charge transfer from graphene to ReS_2 occurred. At the same time, the electrons doping to E_c of ReS_2 also hindered the charge transfer from HOMO of CuPc to ReS_2 (Fig. 5(a)), so the Raman enhancement effect was decreased, and the degree of anisotropy was also reduced.

3 Conclusion

In-plane anisotropic Raman enhancement effect can be modulated and even disappears by the electrons doping of anisotropic 2D ReS_2. The probability of charge transfer from HOMO of CuPc molecules to the conduction band (E_c) of layered ReS_2 was reduced due to the electrons doping to E_c by gold. Hence, the difference between enhancement of molecules with different orientation was diminished and the degree of anisotropy in enhancement disappeared. By increasing the layer number of ReS_2, the degree of anisotropy gradually returned to that without gold. KPFM measurements confirmed the electrons doping of ReS_2. Moreover, graphene was used to replace gold film, and the intermediate degree of anisotropy of Raman enhancement was observed, indicating a moderate doping level of ReS_2 by graphene. The results indicate that, carriers doping can effectively change the probability of charge transfer between materials and molecules, and in-plane anisotropic Raman enhancement of 2D materials with low symmetry can sensitively reflect the doping level of the materials.

4 Experimental

4.1 Sample preparation and characterization

4.1.1 *ReS_2/Au heterostructure*

ReS_2 was prepared by mechanical exfoliation onto a freshly cleaved fluorophlogopite mica substrate. The ReS_2 sample was characterized by optical microscopy, atom force microscopy and Raman spectroscopy. A gold film was then deposited onto ReS_2 at a rate of about 0.1 Å/s and at a pressure of about 10^{-3} Pa by vacuum thermal evaporation. The typical thickness was around 400 Å. Next, the poly(methyl methacrylate) (PMMA) film was then fabricated by spin-coating and dried at 170 °C for 3 min. After that, the as-prepared PMMA/Au/ReS_2 sample was flipped vertically and transferred onto a SiO_2/Si (300 nm) substrate. Owing to the hydrophilicity difference of ReS_2 and fluorophlogopite mica, water was used as the etchant to delaminate ReS_2 monolayer from mica substrate.

4.1.2 *ReS_2/graphene heterostructure*

Graphene and ReS_2 were prepared by chemical vapor deposition, and transferred to a SiO_2/Si (300 nm) substrate one by one. After that, the as-prepared ReS_2/graphene heterostructure was annealed in a 300 standard-state cubic centimeter per minute (sccm) Ar and 50 sccm H_2 atmosphere at 300 °C for 1 h.

4.1.3 *Deposition of CuPc molecules*

CuPc molecules were deposited on the substrate by a standard thermal evaporator. The base pressure for deposition was about 10^{-3} Pa. The evaporation current was about 66 A. The deposition thickness of the CuPc molecule was monitored by using a quartz crystal monitor. The typical thickness was around 3 Å.

4.2 Raman measurements

The Raman measurement was carried out using a Horiba-Jobin Yvon system with a 632.8 nm He–Ne laser line. The laser power was around 1 mW on the sample and a 100× objective was used to focus the laser. The size of the laser spot on the sample was around 1 μm^2. The exposure time for a Raman spectrum was 10 s. To study the polarization dependence of the enhanced Raman spectra, ARPRS was performed under parallel polarization configuration (the polarization of the incident laser parallel to that of the scattered light). The Raman peaks were fitted by a Lorenzian-Gaussion function using the LabSpec software to obtain the Raman peak positions, intensities and full widths at the half-maximum.

4.3 KPFM measurements

The KPFM measurement was carried out using Bruker Dimension Icon system, and the KPFM tip (aluminum (Al)-coated Si tip) was calibrated on a HOPG surface (work function 4.6 eV), and the work functions of the tip and the gold surface were found to be 4.816 and 4.647 eV, respectively. The average ΔV_{CPD} values on the gold film, fewlayer and multilayer ReS_2 flakes were obtained at 322.3, 160.5 and 142.4 mV, respectively. Since ΔV_{CPD} is the difference in the work function between the KPFM tip and the sample, the work function values of the BP and ReS_2 can be calculated using the following equation: $\Phi_S = \Phi_{tip} - \Delta V_{CPD}$, where Φ_S and Φ_{tip} are the work functions of the samples (ReS_2) and the KPFM tip, respectively.

Acknowledgements

The authors thank J. Guan and B. Ma for the vacuum thermal deposition, L. Sun for providing the graphene sample, and S. Jiang for the CVD-grown ReS_2 sample. This work was supported by the National Natural Science Foundation of China (Nos. 51432002, 51720105003, 21790052, 11374355 and 21573004), the Ministry of Science and Technology of China (Nos. 2016YFA0200100 and 2015CB932400), and the Beijing Municipal Science and Technology Project (No. Z161100002116026).

Electronic Supplementary Material: Supplementary material (AFM images of gold film; Raman spectra of CuPc molecules and ReS_2 on different substrates; optical and AFM images of ReS_2 flakes with different thicknesses; angular dependent normalized Raman spectra of gold modulated ReS_2 with different thicknesses; optical images and Raman spectra of monolayer ReS_2 flakes on SiO_2/Si and graphene; angular dependent normalized Raman spectra of ReS_2 flakes on SiO_2/Si and graphene) is available in the online version of this article at https://doi.org/10.1007/s12274-018-2254-y.

References

[1] Liu, H.; Neal, A. T.; Zhu, Z.; Luo, Z.; Xu, X. F.; Tománek, D.; Ye, P. D. Phosphorene: An unexplored 2D semiconductor with a high hole mobility. *ACS Nano* **2014**, *8*, 4033–4041.

[2] Xia, F. N.; Wang, H.; Jia, Y. C. Rediscovering black phosphorus as an anisotropic layered material for optoelectronics and electronics. *Nat. Commun.* **2014**, *5*, 4458.

[3] Wang, X. M.; Jones, A. M.; Seyler, K. L.; Tran, V.; Jia, Y. C.; Zhao, H.; Wang, H.; Yang, L.; Xu, X. D.; Xia, F. N. Highly anisotropic and robust excitons in monolayer black phosphorus. *Nat. Nanotechnol.* **2015**, *10*, 517–521.

[4] Shi, G. S.; Kioupakis, E. Anisotropic spin transport and strong visible-light absorbance in few-layer SnSe and GeSe. *Nano Lett.* **2015**, *15*, 6926–6931.

[5] Yang, S. X.; Liu, Y.; Wu, M. H.; Zhao, L. D.; Lin, Z. Y.; Cheng, H. C.; Wang, Y. L.; Jiang, C. B.; Wei, S. H.; Huang, L. et al. Highly-anisotropic optical and electrical properties in layered SnSe. *Nano Res.* **2018**, *11*, 554–564.

[6] Ho, C. H.; Huang, Y.S.; Tiong, K. K.; Liao, P. C. In-plane anisotropy of the optical and electrical properties of layered ReS_2 crystals. *J. Phys.*:

Condens. Matter **1999**, *11*, 5367–5375.
[7] Liu, E. F.; Fu, Y. J.; Wang, Y. J.; Feng, Y. Q.; Liu, H. M.; Wan, X. G.; Zhou, W.; Wang, B. G.; Shao, L. B.; Ho, C. H. et al. Integrated digital inverters based on two-dimensional anisotropic ReS_2 field-effect transistors. *Nat. Commun.* **2015**, *6*, 6991.
[8] Hafeez, M.; Gan, L.; Li, H. Q.; Ma, Y.; Zhai, T. Y. Chemical vapor deposition synthesis of ultrathin hexagonal $ReSe_2$ flakes for anisotropic raman property and optoelectronic application. *Adv. Mater.* **2016**, *28*, 8296–8301.
[9] Qiao, J. S.; Kong, X.H.; Hu, Z. X.; Yang, F.; Ji, W. High-mobility transport anisotropy and linear dichroism in few-layer black phosphorus. *Nat. Commun.* **2014**, *5*, 4475.
[10] Yuan, H. T.; Liu, X. G.; Afshinmanesh, F.; Li, W.; Xu, G.; Sun, J.; Lian, B.; Curto, A. G.; Ye, G. J.; Hikita, Y. et al. Polarization-sensitive broadband photodetector using a black phosphorus vertical p–n junction. *Nat. Nanotechnol.* **2015**, *10*, 707–713.
[11] Tran, V.; Soklaski, R.; Liang, Y. F.; Yang, L. Layer-controlled band gap and anisotropic excitons in few-layer black phosphorus. *Phys. Rev. B* **2014**, *89*, 235319.
[12] Mao, N. N.; Tang, J. Y.; Xie, L. M.; Wu, J. X.; Han, B. W.; Lin, J. J.; Deng, S. B.; Ji, W.; Xu, H.; Liu, K. H. et al. Optical anisotropy of black phosphorus in the visible regime. *J. Am. Chem. Soc.* **2016**, *138*, 300–305.
[13] Huang, S. X.; Tatsumi, Y.; Ling, X.; Guo, H. H.; Wang, Z. Q.; Watson, G.; Puretzky, A. A.; Geohegan, D. B.; Kong, J.; Li, J. et al. In-plane optical anisotropy of layered gallium telluride. *ACS Nano* **2016**, *10*, 8964–8972.
[14] Tian, Z.; Guo, C. L.; Zhao, M. X.; Li, R. R.; Xue, J. M. Two-dimensional SnS: A phosphorene analogue with strong in-plane electronic anisotropy. *ACS Nano* **2017**, *11*, 2219–2226.
[15] Liu, X. L.; Ryder, C. R.; Wells, S. A.; Hersam, M. C. Resolving the in-plane anisotropic properties of black phosphorus. *Small Methods* **2017**, *1*, 1700143.
[16] Aslan, O. B.; Chenet, D. A.; van der Zande, A. M.; Hone, J. C.; Heinz, T. F. Linearly polarized excitons in single- and few-layer ReS_2 crystals. *ACS Photonics* **2016**, *3*, 96–101.
[17] Zhang, S. S.; Zhang, N.; Zhao, Y.; Cheng, T.; Li, X. B.; Feng, R.; Xu, H.; Liu, Z. R.; Zhang, J.; Tong, L. M. Spotting the differences in two-dimensional materials-the Raman scattering perspective. *Chem. Soc. Rev.* **2018**, *47*, 3380.
[18] Wu, J. X.; Mao, N. N.; Xie, L. M.; Xu, H.; Zhang, J. Identifying the crystalline orientation of black phosphorus using angle-resolved polarized Raman spectroscopy. *Angew. Chem., Int. Ed.* **2015**, *127*, 2396–2399.
[19] Mao, N. N.; Zhang, S. Q.; Wu, J. X.; Zhang, J.; Tong, L. M. Lattice vibration and Raman scattering in anisotropic black phosphorus crystals. *Small Methods* **2018**, *2*, 1700409.
[20] Qiao, X. F.; Wu, J. B.; Zhou, L. W.; Qiao, J. S.; Shi, W.; Chen, T.; Zhang, X.; Zhang, J.; Ji, W.; Tan, P. H. Polytypism and unexpected strong interlayer coupling in two-dimensional layered ReS_2. *Nanoscale* **2016**, *8*, 8324–8332.
[21] Zhao, H.; Wu, J. B.; Zhong, H. X.; Guo, Q. S.; Wang, X. M.; Xia, F. N.; Yang, L.; Tan, P. H.; Wang, H. Interlayer interactions in anisotropic atomically thin rhenium diselenide. *Nano Res.* **2015**, *8*, 3651–3661.
[22] Zhang, E. Z.; Jin, Y. B.; Yuan, X.; Wang, W. Y.; Zhang, C.; Tang, L.; Liu, S. S.; Zhou, P.; Hu, W. D.; Xiu, F. X. ReS_2-based field-effect transistors and photodetectors. *Adv. Funct. Mater.* **2015**, *25*, 4076–4082.
[23] Yang, Y. S.; Liu, S. C.; Yang, W.; Li, Z. B.; Wang, Y.; Wang, X.; Zhang, S. S.; Zhang, Y.; Long, M. S.; Zhang, G. M. et al. Air-stable in-plane anisotropic $GeSe_2$ for highly polarization-sensitive photodetection in short wave region. *J. Am. Chem. Soc.* **2018**, *140*, 4150–4156.
[24] Liu, E. F.; Long, M. S.; Zeng, J. W.; Luo, W.; Wang, Y. J.; Pan, Y. M.; Zhou, W.; Wang, B. G.; Hu, W. D.; Ni, Z. H. et al. High responsivity phototransistors based on few-layer ReS_2 for weak signal detection. *Adv. Funct. Mater.* **2016**, *26*, 1938–1944.
[25] Hong, T.; Chamlagain, B.; Lin, W. Z.; Chuang, H. J.; Pan, M. H.; Zhou, Z. X.; Xu, Y. Q. Polarized photocurrent response in black phosphorus field-effect transistors. *Nanoscale* **2014**, *6*, 8978–8983.
[26] Zhang, E. Z.; Wang, P.; Li, Z.; Wang, H. F.; Song, C. Y.; Huang, C.; Chen, Z. G.; Yang, L.; Zhang, K. T.; Lu, S. H. et al. Tunable ambipolar polarization-sensitive photodetectors based on high-anisotropy $ReSe_2$ nanosheets. *ACS Nano* **2016**, *10*, 8067–8077.
[27] Li, X. B.; Cui, F. F.; Feng, Q. T.; Wang, G.; Xu, X. S.; Wu, J. X.; Mao, N. N.; Liang, X.; Zhang, Z. Y.; Zhang, J. et al. Controlled growth of large-area anisotropic ReS_2 atomic layer and its photodetector application. *Nanoscale* **2016**, *8*, 18956–18962.
[28] Friemelt, K.; Lux-Steiner, M. C.; Bucher, E. Optical properties of the layered transition-metal-dichalcogenide ReS_2: Anisotropy in the van der Waals plane. *J. Appl. Phys.* **1993**, *74*, 5266–5268.
[29] Ho, C. H.; Huang, Y. S.; Tiong, K. K. In-plane anisotropy of the optical and electrical properties of ReS_2 and $ReSe_2$ layered crystals. *J. Alloy. Compd.* **2001**, *317–318*, 222–226.
[30] Lin, Y. C.; Komsa, H. P.; Yeh, C. H.; Björkman, T.; Liang, Z. Y.; Ho, C. H.; Huang, Y. S.; Chiu, P. W.; Krasheninnikov, A. V.; Suenaga, K. Single-layer ReS_2: Two-dimensional semiconductor with tunable in-plane anisotropy. *ACS Nano* **2015**, *9*, 11249–11257.
[31] Avsar, A.; Vera-Marun, I. J.; Tan, J. Y.; Watanabe, K.; Taniguchi, T.; Castro Neto, A. H.; Öezyilmaz, B. Air-stable transport in graphene-contacted, fully encapsulated ultrathin black phosphorus-based field-effect transistors. *ACS Nano* **2015**, *9*, 4138–4145.
[32] Tongay, S.; Sahin, H.; Ko, C.; Luce, A.; Fan, W.; Liu, K.; Zhou, J.; Huang, Y. S.; Ho, C. H.; Yan, J. Y. et al. Monolayer behaviour in bulk ReS_2 due to electronic and vibrational decoupling. *Nat. Commun.* **2014**, *5*, 3252.
[33] Liu, E. F.; Fu, Y. J.; Wang, Y. J.; Feng, Y. Q.; Liu, H. M.; Wan, X. G.; Zhou, W.; Wang, B. G.; Shao, L. B.; Ho, C. H. et al. Integrated digital inverters based on two-dimensional anisotropic ReS_2 field-effect transistors. *Nat. Commun.* **2015**, *6*, 6991.
[34] Liu, F. C.; Zheng, S. J.; He, X. X.; Chaturvedi, A.; He, J. F.; Chow, W. L.; Mion, T. R.; Wang, X. L.; Zhou, J. D.; Fu, Q. D. et al. Highly sensitive detection of polarized light using anisotropic 2D ReS_2. *Adv. Funct. Mater.* **2016**, *26*, 1169–1177.
[35] Lin, J. J.; Liang, L. B.; Ling, X.; Zhang, S. Q.; Mao, N. N.; Zhang, N.; Sumpter, B. G.; Meunier, V.; Tong, L. M.; Zhang, J. Enhanced Raman scattering on in-plane anisotropic layered materials. *J. Am. Chem. Soc.* **2015**, *137*, 15511–15517.
[36] Miao, P.; Qin, J. K.; Shen, Y. F.; Su, H. M.; Dai, J. F.; Song, B.; Du, Y. C.; Sun, M. T.; Zhang, W.; Wang, H. L. et al. Unraveling the Raman enhancement mechanism on 1T′-phase ReS_2 nanosheets. *Small* **2018**, *14*, 1704079.
[37] Çakir, D.; Sahin, H.; Peeters, F. M. Doping of rhenium disulfide monolayers: A systematic first principles study. *Phys. Chem. Chem. Phys.* **2014**, *16*, 16771–16779.
[38] Kim, J.; Baik, S. S.; Ryu, S. H.; Sohn, Y.; Park, S.; Park, B. G.; Denlinger, J.; Yi, Y.; Choi, H. J.; Kim, K. S. Observation of tunable band gap and anisotropic Dirac semimetal state in black phosphorus. *Science* **2015**, *349*, 723–726.
[39] Qin, J. K.; Shao, W. Z.; Xu, C. Y.; Li, Y.; Ren, D. D.; Song, X. G.; Zhen, L. Chemical vapor deposition growth of degenerate p-type mo-doped ReS_2 films and their homojunction. *ACS Appl. Mater. Interfaces* **2017**, *9*, 15583–15591.
[40] Jing, Y.; Tang, Q.; He, P.; Zhou, Z.; Shen, P. W. Small molecules make big differences: Molecular doping effects on electronic and optical properties of phosphorene. *Nanotechnology* **2015**, *26*, 095201.
[41] Shim, J.; Oh, S.; Kang, D. H.; Jo, S. H.; Ali, M. H.; Choi, W. Y.; Heo, K.; Jeon, J.; Lee, S.; Kim, M. et al. Phosphorene/rhenium disulfide heterojunction-based negative differential resistance device for multi-valued logic. *Nat. Commun.* **2016**, *7*, 13413.
[42] Yang, Z. B.; Hao, J. H. Recent progress in black-phosphorus-based heterostructures for device applications. *Small Methods* **2018**, *2*, 1700296.
[43] Yang, L. M.; Majumdar, K.; Liu, H.; Du, Y. C.; Wu, H.; Hatzistergos, M.; Hung, P. Y.; Tieckelmann, R.; Tsai, W.; Hobbs, C. et al. Chloride molecular doping technique on 2D materials: WS_2 and MoS_2. *Nano Lett.* **2014**, *14*, 6275–6280.
[44] Wolverson, D.; Crampin, S.; Kazemi, A. S.; Ilie, A.; Bending, S. J. Raman spectra of monolayer, few-layer, and bulk $ReSe_2$: An anisotropic layered semiconductor. *ACS Nano* **2014**, *8*, 11154–11164.
[45] Lombardi, J. R.; Birke, R. L. Theory of surface-enhanced Raman scattering in semiconductors. *J. Phys. Chem. C* **2014**, *118*, 11120–11130.
[46] Chenet, D. A.; Aslan, O. B.; Huang, P. Y.; Fan, C.; van der Zande, A. M.; Heinz, T. F.; Hone, J. C. In-plane anisotropy in mono-and few-layer ReS_2 probed by Raman spectroscopy and scanning transmission electron microscopy. *Nano Lett.* **2015**, *15*, 5667–5672.
[47] Basova, T. V.; Kolesov, B. A. Raman spectra of copper phthalocyanin: Experiment and calculation. *J. Struct. Chem.* **2000**, *41*, 770–777.
[48] Liu, Z. Q.; Zhang, X. X.; Zhang, Y. X.; Jiang, J. H. Theoretical investigation of the molecular, electronic structures and vibrational spectra of a series of first transition metal phthalocyanines. *Spectrochim. Acta. A: Mol. Biomol. Spectrosc.* **2007**, *67*, 1232–1246.
[49] Basova, T. V.; Kiselev, V. G.; Schuster, B. E.; Peisert, H.; Chassé, T. Experimental and theoretical investigation of vibrational spectra of copper phthalocyanine: Polarized single-crystal Raman spectra, isotope effect and

DFT calculations. *J. Raman Spectrosc*. **2009**, *40*, 2080–2087.
[50] Barros, E. B.; Dresselhaus, M. S. Theory of Raman enhancement by two-dimensional materials: Applications for graphene-enhanced Raman spectroscopy. *Phys. Rev. B* **2014**, *90*, 035443.
[51] Han, X. X.; Ji, W.; Zhao, B.; Ozaki, Y. Semiconductor-enhanced Raman scattering: Active nanomaterials and applications. *Nanoscale* **2017**, *9*, 4847–4861.
[52] Hegner, M.; Wagner, P.; Semenza, G. Ultralarge atomically flat template-stripped Au surfaces for scanning probe microscopy. *Surf. Sci*. **1993**, *291*, 39–46.
[53] Schatz, G. C.; Young, M. A.; van Duyne, R. P. Electromagnetic mechanism of SERS. In *Surface-Enhanced Raman Scattering*: *Physics and Applications*. Kneipp, K.; Moskovits, M.; Kneipp, H., Eds.; Springer: Berlin, Heidelberg, 2006; pp 19–45.
[54] Feng, Y. Q.; Zhou, W.; Wang, Y. J.; Zhou, J.; Liu, E. F.; Fu, Y. J.; Ni, Z. H.; Wu, X. L.; Yuan, H. T.; Miao, F. et al. Raman vibrational spectra of bulk to monolayer ReS_2 with lower symmetry. *Phys. Rev. B* **2015**, *92*, 054110.
[55] Buscema, M.; Steele, G. A.; van der Zant, H. S. J.; Castellanos-Gomez, A. The effect of the substrate on the Raman and photoluminescence emission of single-layer MoS_2. *Nano Res*. **2014**, *7*, 561–571.
[56] McCreary, A.; Simpson, J. R.; Wang, Y. X.; Rhodes, D.; Fujisawa, K.; Balicas, L.; Dubey, M.; Crespi, V. H.; Terrones, M.; Walker, A. R. H. Intricate resonant Raman response in anisotropic ReS_2. *Nano Lett*. **2017**, *17*, 5897–5907.
[57] Ferrari, A. C. Raman spectroscopy of graphene and graphite: Disorder, electron-phonon coupling, doping and nonadiabatic effects. *Solid State Commun*. **2007**, *143*, 47–57.
[58] Takahashi, T.; Tokailin, H.; Sagawa, T. Angle-resolved ultraviolet photo-electron spectroscopy of the unoccupied band structure of graphite. *Phys. Rev. B* **1985**, *32*, 8317–8324.
[59] Park, J. Y.; Joe, H. E.; Yoon, H. S.; Yoo, S.; Kim, T.; Kang, K.; Min, B. K.; Jun, S. C. Contact effect of ReS_2/metal interface. *ACS Appl. Mater. Interfaces* **2017**, *9*, 26325–26332.
[60] Rivière, J. C. The work function of gold. *Appl. Phys. Lett*. **1966**, *8*, 172.
[61] Cui, X. D.; Freitag, M.; Martel, R.; Brus, L.; Avouris, P. Controlling energy-level alignments at carbon nanotube/Au contacts. *Nano Lett*. **2003**, *3*, 783–787.
[62] Chu, C. W.; Shrotriya, V.; Li, G.; Yang, Y. Tuning acceptor energy level for efficient charge collection in copper-phthalocyanine-based organic solar cells. *Appl. Phys. Lett*. **2006**, *88*, 153504.
[63] Jung, N.; Kim, N.; Jockusch, S.; Turro, N. J.; Kim, P.; Brus, L. Charge transfer chemical doping of few layer graphenes: Charge distribution and band gap formation. *Nano Lett*. **2009**, *9*, 4133–4137.